Leakage Current Property of Cation-substituted $BiFeO_3$ Ceramics

Kazutomo Abe, Noriyoshi Sakai, Junichi Takahashi, Hidenobu Itoh[1], Nobuyasu Adachi[2] and Toshitaka Ota[2]

Division of Materials Chemistry, Faculty of Engineering, Hokkaido University, Kita 13, Nishi 8, Kita-ku, Sapporo, Hokkaido, 060-8628, Japan

[1]Department of Materials Science, Kitami Institute of Technology, koen-cho 165, Kitami, Hokkaido, 090-8507, Japan

[2]Ceramics Research Laboratory, Nagoya Institute of Technology, Asahigaoka 10-6-29, Tajimi, Gifu, 507-0071, Japan

Key Words; multiferroic material, oxide, leakage current property, $BiFeO_3$, co-doping

Abstract

Cation-doped $BiFeO_3$ ceramics were fabricated by sintering coprecipitated and calcined powders at 700° - 900°C to study the effect of cation doping on the leakage current property of the sintered samples. Among the dopants examined in this study, Ti^{4+}, Sn^{4+} or Zr^{4+} doping was found to reduce effectively the leakage current of the samples. Especially, a remarkable decrease in the leakage current density was achieved at 10% of the Ti^{4+} doping, which also resulted in the structure change from rhombohedral to cubic. Co-doping of the Ti^{4+}/Zn^{2+} ions or Ti^{4+}/Ni^{2+} ions brought about the substantial reduction in the leakage current density of the bulk samples by about four or five orders of magnitude at a small doping amount of 2%. This could be explained by a combined effect of the Ti^{4+} doping, which basically contribute to the decreasing number of oxygen vacancies in the sample, and the Zn^{2+} or Ni^{2+} doping, which might assist the homogeneous substitution of the Ti^{4+} ions for the Fe^{3+}-sites.

1. Introduction

$BiFeO_3$ (BFO) is a remarkably valuable material that is simultaneously ferroelectric and anti-ferromagnetic in the same phase at room temperature (RT).[1,2] Coupling between both ferroic orders could offer new applications to the ultimate memory devices.[1, 3-6] However, there are two major obstacles to be overcome to achieve the practical usage of BFO-based devices. One obstacle is large leakage current and the other is very weak magnetization induced from G-type antiferromagnetism.[7-12] Especially, the highly electrical conductive nature of BFO makes it difficult to provide excellent ferroelectric properties. In BFO, oxygen vacancies could be produced by the vaporization of Bi or the presence of lower valence Fe^{2+} ions, which leads to the formation of a trap level at 0.6 eV below the bottom edge of the conduction band.[13] In lower electric field region, the electric current in BFO might be transferred by space charge limited mechanism after ohmic conduction, whereas it would be predominantly governed by one of the following mechanisms, Poole-Frenkel conduction[14], Schottky conduction[14], and field-assisted ionic conduction[15] under higher electric field.

Two different approaches have been conducted to reduce the leakage current in BFO. One is a procedure for directly lowering the number of the oxygen vacancies by the injection of oxide ions[16] and doping of rare-earth cations to the Bi^{3+}-sites.[8,17-20] The other method is to compensate the unbalanced ionic charge induced by the formation of oxygen vacancies. Thus cation substitution with higher valences for the Fe^{3+}-sites in BFO has been studied.[7,9,21] Most of these studies have been conducted for thin films and therefore there have been a limited number of studies on the BFO bulk samples. This limitation seems to come from the difficulties in fabricating dense and single-phase BFO ceramics at relatively lower temperature and the fact that the resulting electrical and magnetic properties strongly depend on processing factors such as the powder characteristics of raw materials and various sintering variables. Particularly, it is very difficult to obtain densified BFO ceramics with compositional homogeneity by sintering at low temperatures. In fact, even for a sol-gel derived powder sintering at 800ºC was required to produce BFO ceramics with a saturated ferroelectric hysteresis loop.[22] It is essentially important to fabricate BFO bulk samples and collect reproducible properties data in order to understand the fundamental physics of BFO materials. In this study, therefore, BFO ceramics were fabricated by low-temperature sintering of coprecipitated and calcined powders, which might be expected to assist the inhibited vaporization of Bi during sintering. Besides, the single-doping and co-doping of aliovalent cations for the Fe^{3+}-sites were made to examine the effect of such cation doping on the leakage property and magnetic structure of the bulk BFO samples.

2. Experimental procedure

Precursor powders to BFO were prepared by quantitative coprecipitation of required cations in an aqueous ammonia solution. Bi_2O_3 and hydrated $Fe(NO_3)_3$ were used for preparing a basic compound of BFO. Hydrated nitrates of Ni, Zn or Mn and Ti, Sn or Zr alkoxides were used as individual sources for cation doping. An aqueous nitrate solution containing given amounts of Bi^{3+}, Fe^{3+} and a cation(s) to be doped was rapidly poured into an excess amount of aqueous ammonia solution to form a solid precipitate. After thoroughly washed with distilled water, the precipitate was dried and then calcined at 500° - 650°C for 4h in air. Green compacts were formed by an uniaxial pressing of the calcined powder at 40 MPa followed by cold isostatic pressing at 100 MPa. Then they were heated up to a fixed temperature of 700° – 900°C at a heating rate of 100°C/h and sintered for 2h. The doping amount was adjusted to be 2, 5 or 10 at% for the Fe sites in the BFO structure.

Solid phase identification and lattice parameter calculation of the sintered BFO samples were conducted by powder X-ray diffractometry (XRD, Rigaku RINT 2200). The microstructure of sintered samples was observed by scanning electron microscopy (SEM, JEOL JSM-6300F). Samples for leakage current measurement were prepared by first polishing a sintered sample until the thickness became less than 200μm and then coating 3-probe type electrodes with Ag-leads. A high resistance meter (ADCMT 8340A) was used for evaluating V-I characteristics of the Ag-coated samples. The magnetic behavior of powdered samples was measured at room temperature by vibrating sample magnetometer (VSM) under magnetic field ranging from 1.5kOe to -1.5kOe.

3. Results and Discussion

3.1. Fabrication and leakage current property of cation-doped BFO ceramics

Sintering conditions were optimized to obtain densified BFO ceramics at temperatures as low as possible. The results are summarized in Table 1 where in the upper columns BFO samples with doping of lower valence or the same cations than Fe^{3+} are listed. Undoped BFO ceramics could be fabricated from a coprecipitated precursor powder by calcination at 500° - 550°C and sintering at 750°C for 2h. From this considerably lower sintering temperature of 750°C, the inhibited Bi vaporization had been expected. Despite of using a very fine coprecipitated powder, however, very small amounts of secondary phases such as $Bi_2Fe_4O_9$ and $Bi_{25}FeO_{29}$ inevitably appeared in the sintered samples[8, 17, 18, 24], as can be seen in Fig.1.

Among lower valence cations doped, Ni^{2+} doping was effective on the densification of BFO ceramics at a lower sintering temperature (700°C). It is unlikely that a liquid phase was formed at such a low temperature in the Bi_2O_3-FeO-NiO system. Probably, mass transport during sintering

might be fairly accelerated by the incorporation of the Ni^{2+} ions. The XRD pattern of the 5% Ni^{2+}-doped BFO sample (Ni-5) depicted in Fig.1 showed that the formation of the secondary phases was considerably suppressed by the Ni^{2+} doping. A similar effect of inhibiting the formation of the secondary phase during sintering was observed for the Zn^{2+} doping. This result suggested that the Ni^{2+} and Zn^{2+} ions would assist the ionic diffusion in BFO to produce compositionally homogeneous bulk ceramics.

Changes in leakage current density (J) with applied electric field (E) are plotted in Fig.2 for BFO samples marked with * in Table 1. It is clearly observed that for the undoped sample a very large current flowed in a low E region, despite that the sample was fabricated by sintering at as low as 750°C. The large leakage current behavior might be attributed to the substantial vaporization of Bi even at 750°C and the presence of the secondary phase of $Bi_2Fe_4O_9$ having a very leaky property.[24] However, the large leakage current of the undoped sample could be lowered by Mn^{3+} and Ni^{2+} doping. The decreasing current density caused by Mn^{3+} doping was already reported for BFO films with somewhat different behaviors.[10, 25, 26] That is, J values of the Mn^{3+}-doped films were higher than those of undoped films in a low E region but they became smaller at higher E as a result of reduced rates of the increasing J. Mn^{3+} doping in this study, however, resulted in reduced J values of the doped BFO samples even in a low E region. From a linear relationship in the log (J) vs log (E) plot for the 5%Mn^{3+}-doped and undoped BFO ceramics, the slopes α in an expression $J \propto E^{\alpha}$ were evaluated to be $\alpha \approx 1.4$ and $\alpha \approx 2.4$, respectively. The decreasing α value for the Mn^{3+}-doped sample might be explained by the formation of carrier trap levels[26]. An increase in the α value ($\alpha \approx$ 5.8) with increasing electric field above 10 kV/cm revealed that the trap levels were completely filled up. Thus, it was clear that very conductive nature of the undoped BFO ceramics was altered to become much resistive one by Mn^{3+} doping as expected[26, 27].

A reduction of J was also observed for the Ni^{2+}-doped BFO ceramics (Fig.2). This result was definitely contrary to that obtained for the Ni^{2+}-doped BFO films, in which the leakage current increased by nearly two orders of magnitude compared to the undoped BFO film.[7] The authors explained the cause of the increasing J by the descriptions that a dominant charge compensation mechanism in the Ni^{2+}-doped BFO was the creation of oxygen vacancies and a higher concentration of oxygen vacancies led to a higher density of free carriers. The different behavior observed in the Ni^{2+}-doped BFO sample fabricated in this study required a different explanation. Considering that Ni^{2+}-doped bulk sample could be fabricated by sintering at a lower temperature with the suppressed formation of the secondary phases in this study, the production of much homogeneous bulk sample might be responsible for the reduced leakage current in the Ni^{2+}-doped BFO ceramics.

As can be seen in Table 1, doping of the Ti^{4+}, Sn^{4+} and Zr^{4+} ions required elevated temperature for the BFO ceramics to be sintered, because of their highly refractive nature. XRD analysis showed that the Ti^{4+} doping brought about the production of a nearly single-phase BFO sample without any additional peaks corresponding to a new Ti^{4+}-containing compound even at a doping amount of 10%. Thus, the Ti^{4+} ions could be substituted up to 10% for the Fe^{3+}-sites in the BFO structure. Concerning the Sn^{4+} or Zr^{4+} doping, diffraction peaks of the secondary phases were appreciably intensified for 10%-doped samples, indicating that the solubility limits of the Sn^{4+} and Zr^{4+} ions are between the doping amount of 5 -10% and less than that of the Ti^{4+} ions. XRD patterns of the Ti^{4+}-doped samples in Fig.1 also indicate that two diffraction peaks of the (104) and (110) planes at $2\theta \approx 31.7°$ and $\approx 32.0°$, respectively, which are distinctly splitted in the rhombohedral structure, appear to beccme a single diffraction peak at the 10% Ti^{4+} doping. This peak change must be correlated to the structure change of BFO from the rhombohedral phase to the high-temperature cubic one.[28] No similar XRD peak change was observed for 10% Sn^{4+}- and Zr^{4+}-doped samples.

In a pure sintered BFO, a substantial number of oxygen vacancies are created to compensate positive charge deficiency caused by the vaporization of Bi and the reduction of the Fe^{3+} ions to Fe^{2+}, resulting in a very large leakage current density of the sample. There have been several reports on the reduction in leakage current in BFO films by the Ti^{4+} doping.[7, 29] X. Qi et al. described from a log (J) $\propto E$ relation obtained for Ti^{4+}-doped BFO films that the electrical conduction process was predominated by field-assisted ionic conduction, which resulted from greatly reduced oxygen vacancies.[7] As shown in Fig.3, doping of the aliovalent cations of Ti^{4+}, Sn^{4+} and Zr^{4+} could more or less result in a substantial decrease in the leakage current of BFO ceramics. Especially, a remarkable effect was demonstrated by Ti^{4+}-doped samples, in which a small leakage current could be obviously retained up to higher E for 10% Ti^{4+}-doped BFO sample. Higher J values observed for Sn^{4+}- and Zr^{4+}- doped samples could be explained by poor densification of bulk samples sintered under the present conditions. The present results revealed that the incorporation of cations having a higher valence than the Fe^{3+} ions could definitely compensate the cation deficiency in the sample to reduce effectively the oxygen vacancies instead of forming the Fe^{2+} ion.

3.2. Effects of Ti^{4+}/Zn^{2+} and Ti^{4+}/Ni^{2+} co-doping on leakage current and magnetic properties

It is interesting to study co-doping effects on the leakage current and magnetic properties of BFO because a synergetic effect might appear from the co-doping of different cations. For example, a combination of La^{3+} doping, which is favorable for stabilizing the perovskite phase, with V^{5+} doping resulted in the enhanced ferroelectric and anti-fatigue properties of BFO ceramics, which might be attributed to the possible crystal lattice distortion and low charge defects (oxygen

vacancies) in the sample.[9] In the present study, it became clear that the leakage current property of BFO ceramics could be considerably improved by Ti^{4+} doping. Therefore, combination of Ti^{4+} doping with Zn^{2+} or Ni^{2+} doping, which could assist the inhibited formation of secondary phases at low-temperature sintering, were examined in this section. Figure 4 shows the leakage current characteristics of the BFO samples modified by co-doping of (A) Ti^{4+}/Zn^{2+} and (B) Ti^{4+}/Ni^{2+} ions, for which the doping amount was adjusted to be 2, 5 and 10 at% (e.g., a 5% Ti^{4+}/Zn^{2+} co-doping demonstrates that both 2.5% Ti^{4+} and 2.5% Zn^{2+} ions are incorporated into the BFO sample.). It can be clearly seen that *J* was remarkably reduced at a small doping amount of 2% for each co-doped BFO sample. For a single doping of the Ti^{4+} ions, a steep increase in *J* below 5 kV/cm and a sudden rise of *J* at ~ 35 kV/cm occurred in the 2% and 5%Ti^{4+}-doped BFO samples, respectively (Fig. 3). The dielectric breakdown observed in these Ti^{4+}-doped samples could be attributed to the inhomogeneous incorporation of the Ti^{4+} ions into the BFO sample. On the contrary, such behavior leading to dielectric breakdown could not be detected for the co-doped samples even at an actual amount of 1% Ti^{4+} doping (a co-doping amount of 2%). Therefore, the role of the Zn^{2+} and Ni^{2+} ions in the co-doping would be basically to promote the homogenized distribution of the Ti^{4+} ions in the sample. The XRD patterns of selected samples are given in Fig.5. It was evident that bulk samples containing a trace amount of the secondary phase could be obtained by sintering at 800 °C when the Ti^{4+}/Zn^{2+} or Ti^{4+}/Ni^{2+} co-doping was employed. This result supported the explanation that the substantially reduced leakage current in the co-doped samples was predominately ascribed to the effect of the Ti^{4+} doping and the coupled Zn^{2+} or Ni^{2+} ions might assist the homogeneous incorporation of the Ti^{4+} ions through enhanced ionic diffusion during sintering.

A difference in the dependence of *J* on doping amount was observed for the co-doped samples. *J* values at higher *E* were gradually lowered in the Ti^{4+}/Zn^{2+} co-doped samples with an increasing amount of the dopant, whereas it was found to be almost independent on doping amount for the 5% and 10% Ti^{4+}/Ni^{2+} co-doped samples. If the *J* value would be dominated by only the oxygen vacancy concentration in a BFO sample, the behavior observed in the Ti^{4+}/Zn^{2+} co-doping could be explained by a decreasing number of oxygen vacancies with an increasing amount of doping cations. However, this was not the case for the 5% and 10% Ti^{4+}/Ni^{2+} co-doped samples. Depending on the cation combination of Ti^{4+}/Zn^{2+} or Ti^{4+}/Ni^{2+}, different defect chemistry and electric structures which are closely correlated to specified *J-E* relations might be built up in each sample. Detailed examination is needed for further discussion.

Magnetization (*M*) vs magnetic field (*H*) curves were measured to examine the effect of the cation doping on the magnetic property of BFO ceramics. The results are demonstrated in Fig.6. In pure BFO, the partially filled 3d orbitals of the Fe^{3+} ions cause G-type antiferromagnetic order and the linear magnetoelectric effect is forbidden in the pure BFO.[11] Zn^{2+}, Ni^{2+} and Mn^{3+} doping

(Fig.6(A)) resulted in an increasing magnetization in an order of $Ni^{2+} \rightarrow Zn^{2+} \rightarrow Mn^{3+}$ without hysteresis in their curves. Remarkably different *M-H* curves can be seen in Fig.6(B) for Ti^{4+}-doped BFO samples. Especially, a clear hysteresis loop indicating the presence of spontaneous magnetization was observed at a doping amount of 5%. An increase in the doping amount up to 10%, on the other hand, led to a smaller hysteresis loop. This change seemed to be correlated to the structure change from rhombohedral system to cubic one (Fig.1). The appearance of spontaneous magnetization by this kind of chemical modification was also reported in a Ti^{4+}-doped BFO sample, in which the modulated antiferromagnetic state was completely destroyed and the remanent magnetization was induced by a minor substitution of the Ti^{4+} ions for the Fe^{3+} ions.[12, 30)] Co-doped samples in Fig.6(C) and 6(D) showed a gradual increase in the remanent magnetization together with an increasing hysteresis loop. Since the rhombohedral structure was retained at a co-doping amount of 10% (Fig.5), the remanent magnetization was found to increase monotonously with an increase in the doping amount for both co-doped samples. The cause of an asymmetric *M-H* curve observed for the 10% Ti^{4+}/Zn^{2+} co-doping was not clear now. The application of a very larger magnetic field might give some information.

Thus, the incorporation of the Ti^{4+} ions into BFO resulted in a magnetic structure change leading to the appearance of spontaneous magnetization, which might be attributed to the spin-canted magnetism in the Ti^{4+}-doped and Ti^{4+}/Zn^{2+} or Ti^{4+}/Ni^{2+} co-doped samples. However, because of limited data on the magnetic properties of the cation-doped BFO ceramics fabricated in this study, it is difficult to discuss in detail a change in the magnetic structure with cation doping. Further studies should be conducted to clarify the optimal composition of a chemically-modified BFO sample which shows spontaneous magnetization and ferroelectricity simultaneously and also to elucidate the spin structure and ferroelectric properties of the modified BFO samples.

4. Conclusion

Doping effects on the leakage current and magnetic properties of BFO ceramics were studied. Coprecipitated powders prepared from homogeneous solutions containing required amounts of Bi^{3+}, Fe^{3+} and doping ions were used to fabricate BFO ceramics. Zn^{2+} and Ni^{2+} doping resulted in the inhibited formation of the secondary phases during low temperature sintering. Doping of the Ti^{4+}, Sn^{4+} or Zr^{4+} ions which has a higher valence than the Fe^{3+} ions effectively suppressed the leakage current density of BFO samples by the reduction in oxygen vacancies. For Ti^{4+}-doped samples, however, a steep current rise was observed at a specific electric field depending on the doping amount up to 5%, which might be due to the inhomogeneous doping of the Ti^{4+} ions in the sintered samples.

Substantial improvement in the leakage current property could be achieved by the co-doping of the Ti^{4+}/Zn^{2+} or Ti^{4+}/Ni^{2+} ions. Especially, a very small co-doping amount of 2% caused a lowering in the leakage current density by about four or five orders of magnitude for each co-doped sample. The enhanced improvement could be attributed to the combined effects of the Ti^{4+} doping, which could contribute to the reduction in the number of oxygen vacancies, and the Zn^{2+} or Ni^{2+} doping, which might assist the homogeneous incorporation of the Ti^{4+} ions by accelerated ionic diffusion during sintering. The appearance of spontaneous magnetization was also confirmed for Ti^{4+}-doped, Ti^{4+}/Zn^{2+} and Ti^{4+}/Ni^{2+} co-doped samples. Doping of the Ti^{4+} ions might build up the spin-canted magnetic structure in the modified BFO ceramics.

References

1) W. Prellier, M. P. Singh, and P. Murugavel: J. Phys.:Condens. Matter **17** (2005) R803.

2) G. A. Smolenskii, V. M. Yudin, E. S. Sher, and Y. E. Stolypin:Sov. Phys. JETP **16** (1963) 622.

3) R. Ramesh and N. A. Spaldin: Nature Mater. **6** (2007) 21.

4) J. F. Scott: Nature Mater. **6** (2007) 256.

5) M. Bibes and A. Barthélémy: IEEE Transactions on Electron Devices **54** (2007) 1003.

6) Y. Tokura: Science **312** (2006) 1481.

7) X. Qi, J. Dho, R. Tomov, M. G. Blamire, and J. L. MacManus-Driscoll: Appl. Phys. Lett. **86** (2005) 062903.

8) S. Zhang, L. Pang, Y. Zhang, M. Lu, and Y. Chen: J. Appl. Phys. **100** (2006) 114108.

9) B. Yu, M. Li, J. Wang, L. Pei, D. Guo, and X. Zhao: J. Phys. D: Appl. Phys. **41** (2008) 185401.

10) T. Kawae, H. Tsuda, H. Naganuma, S. Yamada, M. Kumeda, S. Okamura, and A. Morimoto: J. J. Appl. Phys. **47** (2008) 7586.

11) V. A. Khomchenko, D. A. Kiselev, M. Kopcewicz, M. Maglione, V. V. Shvartsman, P. Borisov, W. Kleemann, A. M. L. Lopes, Y. G. Pogorelov, J. P. Araujo, R. M. Rubinger, N. A. Sobolev, J. M. Vieira, and A. L. Kholkin: J. Magnetism and Magnetic Mater. **321** (2009) 1692.

12) I. O. Troyanchuk, M. V. Bushinsky, A. N. Chobot, O. S. Mantytskaya, and N. V. Tereshko: JETP Lett. **89** (2009) 180.

13) S. J. Clark and J. Robertson: Appl. Phys. Lett. **94** (2009) 022902.

14) M. Iwamoto:Yuukizetsuennzairyou no saisenntann, CMC pub. (2007) p.145-166.

15) P. J. Harrop: Dielectrics (Butterworths, London, 1972) p.51-53

16) X. H. Xiao, J. Zhu, Y. R. Li, W. B. Luo, B. F. Yu, L. X. Fan, F. Ren, C. Liu, and C. Z. Jiang: J. Phys. D: Appl. Phys. **40** (2007) 5775.

17) K. S. Nalwa and A. Garg: J. Appl. Phys. **103** (2008) 044101.

18) H. Uchida, R. Ueno, H. Nakaki, H. Funakubo, and S. Koda: Jpn. J. Appl. Phys. **44** (2005) L561.

19) C. Lee and J. Wu: Electrochem. Solid-State Lett. **18** (2007) G58.

20) G. D. Hu, X. Cheng, W. B. Wu, and C. H. Yang:Appl. Phys. Lett. **91** (2007) 232909.

21) A. Z. Simões, R. F. Pianno, E. C. Aguiar, E. Longo and J. A. Varela: J. Alloys Comp. **479** (2009) 274.

22) F. Chen, Q. F. Zhang, J. H. Li, Y. J. Qi, C. J. Lu, X. B. Chen, X. M. Ren, and Y. Zhao: Appl. Phys. Lett. **89** (2006) 092910.

23) A. K. Pradhan, K. Zhang, D. Hunter, J. B. Dadson, G. B. Loutts, P. Bhattacharya, R. Katiyar, J. Zhang, D. J. Selmyer, U. N. Roy, and A. Burger: J. Appl. Phys. **97** (2005) 093903.

24) J. H. Miao, T. Fang, H. Chung, and C. Yang: J. Am. Ceram. Soc. **92** [11] (2009) 2762.

25) S. K. Singh, H. Ishiwara, K. Sato, and K. Maruyama: J. Appl. Phys. **102** (2007) 094109.

26) K. Kawae, Y. Terauchi, H. Tsuda, M. Kumeda, and A. Morimoto: Appl. Phys. Lett. **94** (2009) 112904.

27) T. Higuchi, T. Hattori, W. Sakamoto, N. Itoh, T. Shimura, T. Yogo, P. Yao, Y. Liu, P. Glans, C. Chang, Z. Wu, and J. Guo: Jpn. J. Appl. Phys. **47** [9] (2008) 7570.

28) M. Azuma, S. Niitaka, N. Hayashi, K. Oka, M. Takano, H. Funakubo, and Y. Shimakawa: Jpn. J. Appl. Phys. **47** [9] (2008) 7579.

29) L. Chen, W. Ren, W. Zhu, Z. Ye, P. Shi, X. Chen, X. Wu, and X. Yao: Thin Solid Films, **518** (2010) 1637.

30) I. Sosnowska, T. Peterrlin-Neumaier and E. Steichele: J. Phys. C **15** (1982) 4835.

Figure captions

Fig.1 XRD profiles of BFO ceramics (A) without dopant and doped with (B) 5% Mn^{3+}, (C) 5% Ni^{2+}, (D) 5% Ti^{4+} and (E) 10% Ti^{4+}. (They were sintered at different temperatures listed in Table 1.)

Fig.2 Leakage current density changes with electric field for BFO samples without dopant and with 5% Zn^{2+}, 5% Ni^{2+} and 5% Mn^{3+} doping

Fig.3 Leakage current density changes with electric field for Sn^{4+}-, Zr^{4+}- and Ti^{4+}-doped BFO samples.

Fig.4 Effect of cation co-doping on leakage current density of sintered BFO samples with (A) Ti^{4+}/Zn^{2+} co-doping and (B) Ti^{4+}/Ni^{2+} co-doping.

Fig.5 XRD patterns of (A) 5% Ti^{4+}/Zn^{2+}, (B) 10% Ti^{4+}/Zn^{2+}, (C) 5%Ti^{4+}/Ni^{2+} and (D) 10% Ti^{4+}/Ni^{2+} co-doped BFO samples.

Fig.6 Magnetization vs magnetic field plots for (A) Zn^{2+}-, Ni^{2+}- and Mn^{3+}-doped, (B) Ti^{4+}-doped, (C) Ti^{4+}/Zn^{2+} co-doped and (D) Ti^{4+}/Ni^{2+} co-doped BFO samples.

Table 1 Bulk density and lattice parameter for cation-doped BFO ceramics fabricated under each sintering condition.

Doping species	Amount (mol%)	Sintering condition [ºC] (Calcining / Sintering)	Density [g/cm^3]	Lattice parameter a [nm]	α [º]
Non	0*	550 / 750	7.86	0.3964	89.44
Mn	2	550 / 750	7.85	—	
	5*	550 / 750	7.68	0.3964	89.44
	10	550 / 750	7.63	0.3961	89.54
Zn	2	550 / 750	7.95	—	
	5*	550 / 750	7.79	0.3967	89.48
Ni	2	550 / 700	7.92	—	
	5*	550 / 700	7.97	0.3965	89.42
Ti	2*	600 / 850	7.40	—	
	5*	600 / 850	7.45	0.3961	89.57
	10*	600 / 900	7.39	0.3955	90.02
Sn	5*	600 / 850	6.95	0.3963	89.41
Zr	5*	600 / 850	6.68	0.3967	89.44

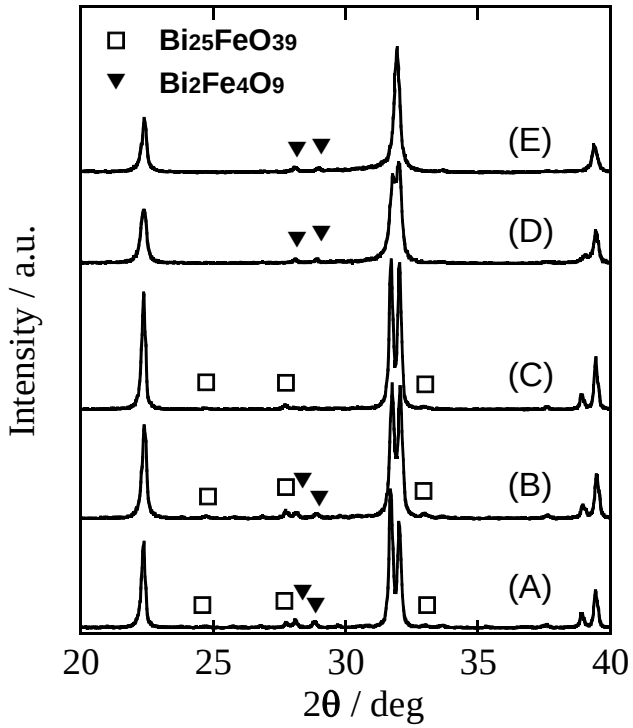

Fig.1 XRD profiles of BFO ceramics (A) without dopant and doped with (B) 5% Mn^{3+}, (C) 5% Ni^{2+}, (D) 5% Ti^{4+} and (E) 10% Ti^{4+}. (They were sintered at different temperatures listed in Table 1.)

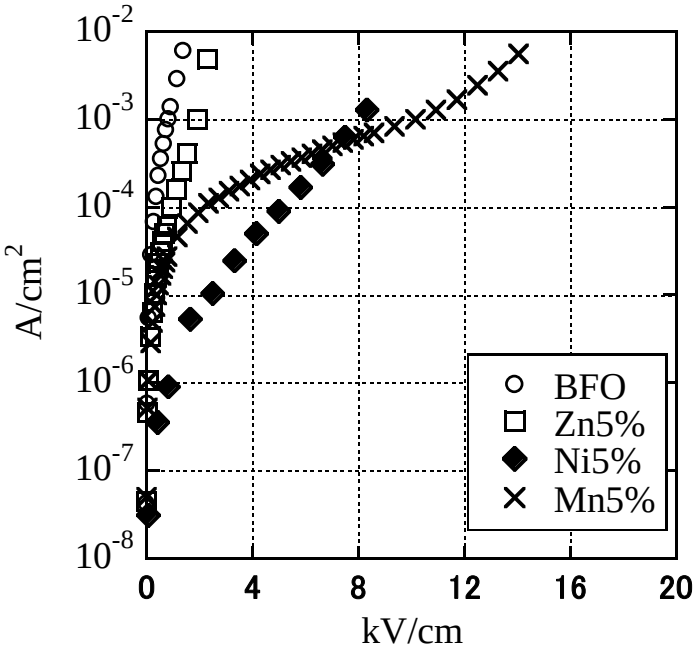

Fig.2 Leakage current density changes with electric field for BFO samples without dopant and with 5% Zn^{2+}, 5% Ni^{2+} and 5% Mn^{3+} doping

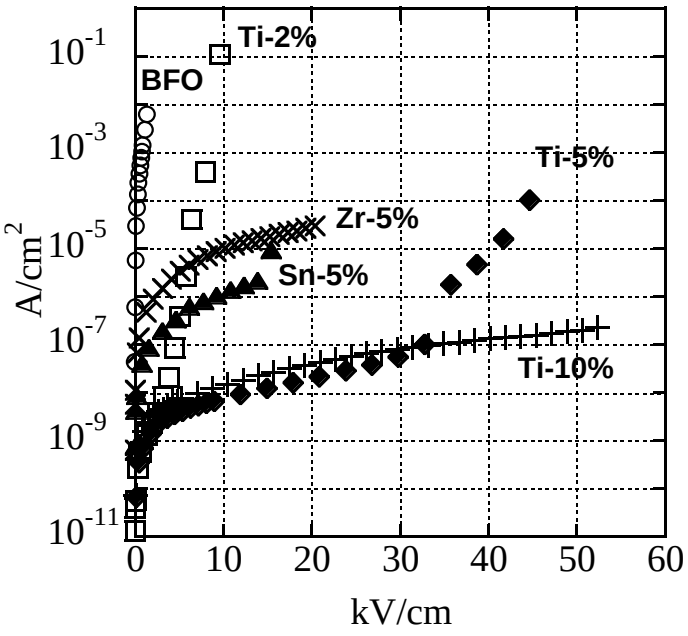

Fig.3 Leakage current density changes with electric field for Sn^{4+}-, Zr^{4+}- and Ti^{4+}-doped BFO samples.

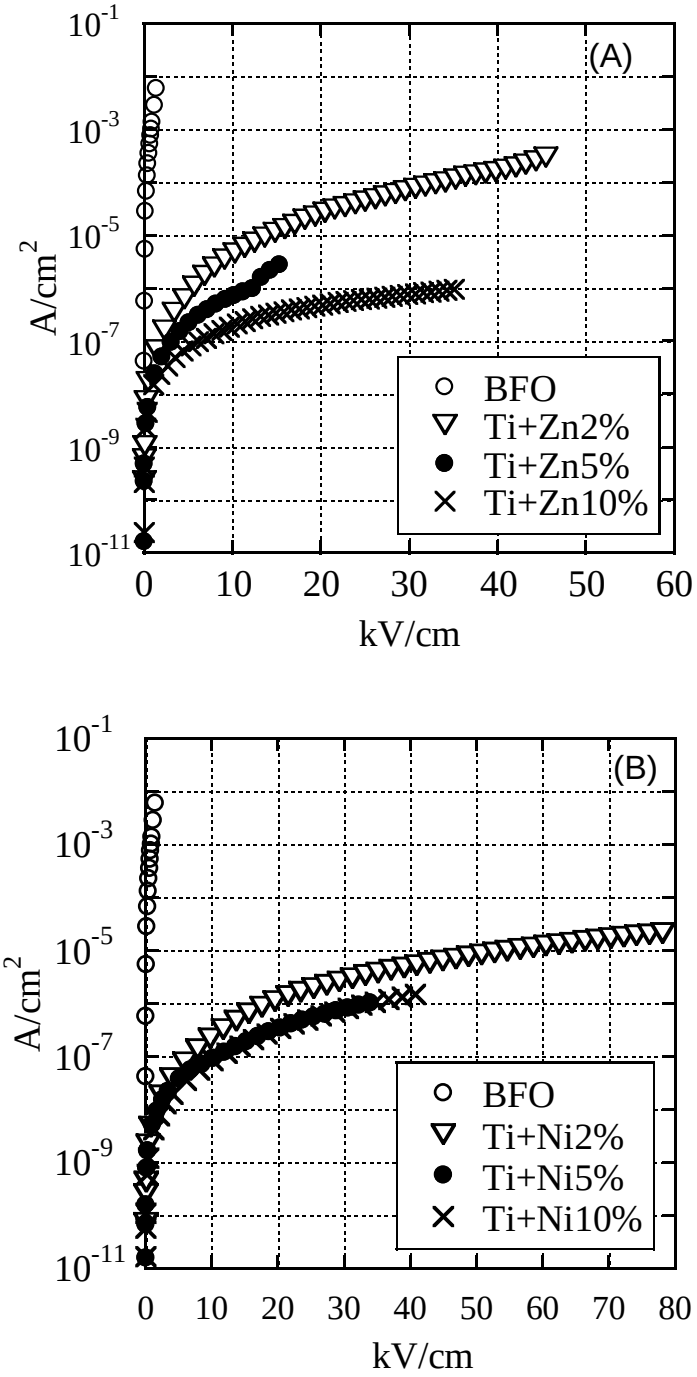

Fig.4 Effect of cation co-doping on leakage current density of sintered BFO samples with (A) Ti^{4+}/Zn^{2+} co-doping and (B) Ti^{4+}/Ni^{2+} co-doping.

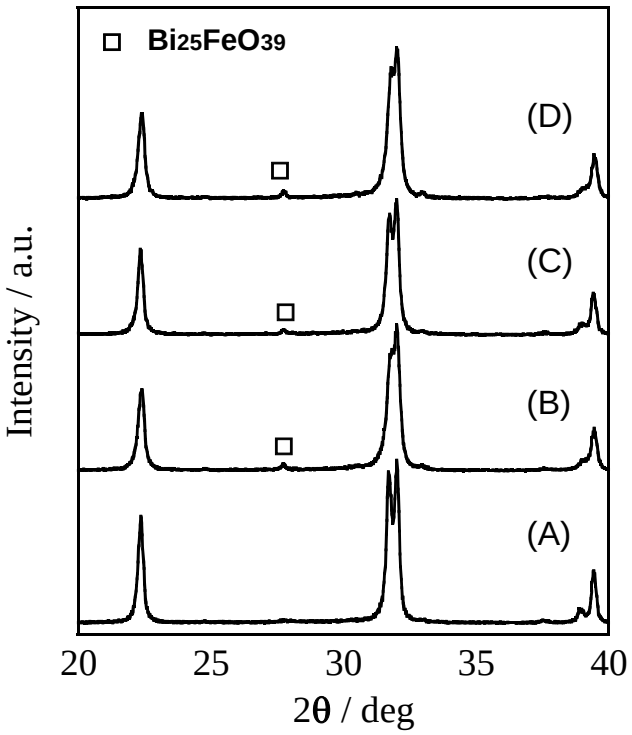

Fig.5 XRD patterns of (A) 5% Ti^{4+}/Zn^{2+}, (B) 10% Ti^{4+}/Zn^{2+}, (C) 5%Ti^{4+}/Ni^{2+} and (D) 10% Ti^{4+}/Ni^{2+} co-doped BFO samples.

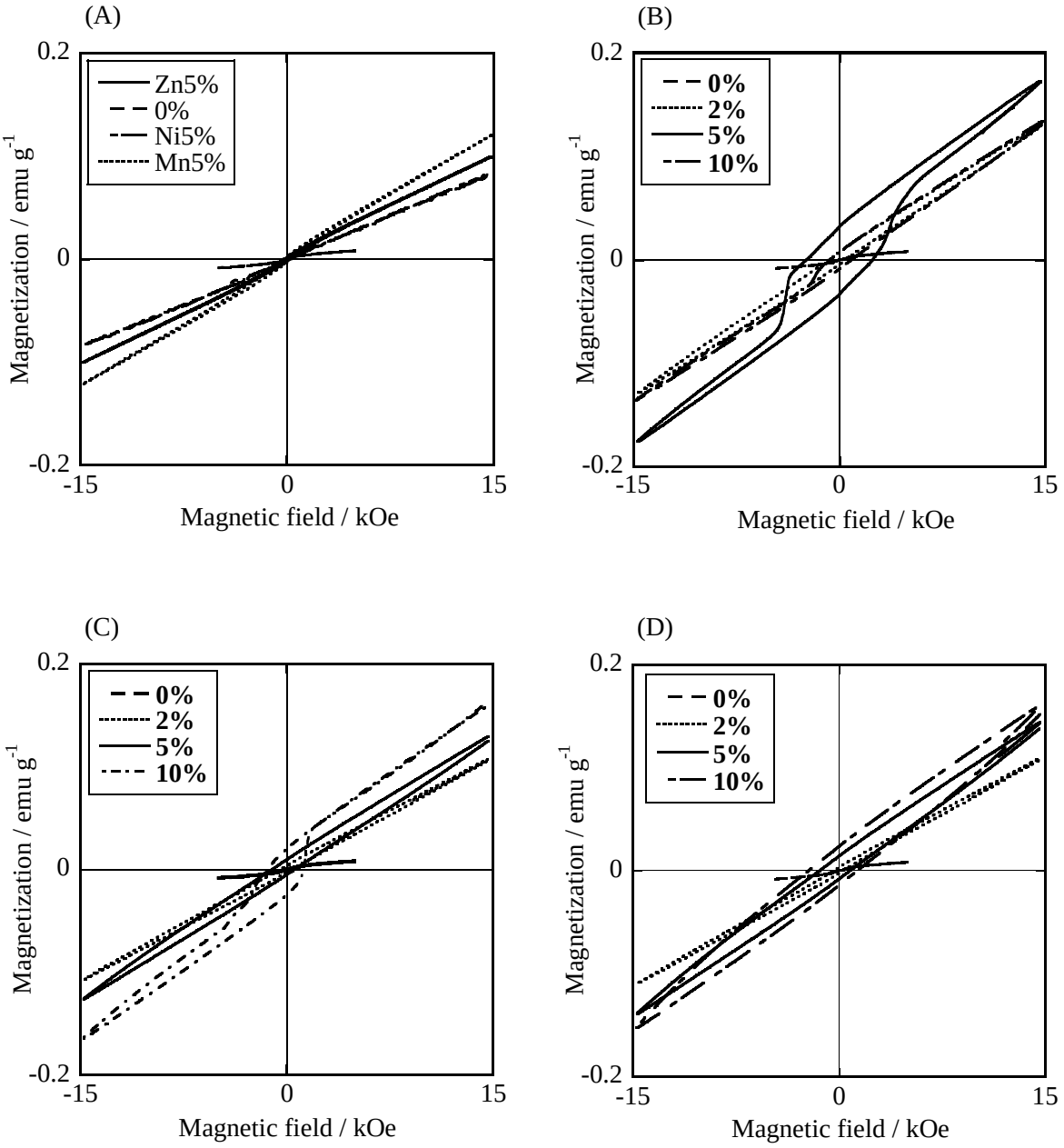

Fig.6 Magnetization vs magnetic field plots for (A) Zn^{2+}-, Ni^{2+}- and Mn^{3+}-doped, (B) Ti^{4+}-doped, (C) Ti^{4+}/Zn^{2+} co-doped and (D) Ti^{4+}/Ni^{2+} co-doped BFO samples.